Electrodeposited Au/FeAu Nanowires with Controlled Porosity

S. Lucatero,[a] W. H. Fowle,[b] and E. J. Podlaha[a,*,z]

aChemical Engineering Department and bBiology Department, Northeastern University, Boston, Massachusetts 02115, USA

Multilayer nanowires tailored with alternating AuFe porous layers and Au nonporous segments were fabricated by galvanic square-wave pulsed electrodeposition from a AuFe cyanide-free electrolyte. Control of porosity and composition was achieved via modulation in pulsed time and applied current density. Nanowires with decreased porosity were observed upon increasing time of the AuFe alloy layer or shifting the applied current density to more negative values. This transition was consistent with an increased amount of material being deposited. The single-step approach presented is less time-consuming than conventionally fabricated nanoporous materials, requiring additional etching of prefabricated solid alloys.
© 2009 The Electrochemical Society. [DOI: 10.1149/1.3238471] All rights reserved.

Nanostructures consisting of alternating nonmagnetic/magnetic thin films with different nobility display unique properties of interest in several technological applications, such as giant magnetoresistance sensors for detecting magnetic storage media[1,2] and biofunctionalized magnetic beads.[3-5] Electrodeposition is a particularly well-suited method for the fabrication of multilayers as thin films and more recently nanowires[6-12] and nanotubes.[13,14] Tailoring multilayers is a particularly convenient way to tune physicochemical properties, such as optical reflectivity, tensile strength, hardness, conductivity, and coercivity.[14-16] In applications such as localized drug delivery, catalysis, and surface reactions in biomicroelectromechanical systems and nanoelectronics, porous substrates displaying high surface-to-volume ratio and controlled porosity are desirable.[12,17-20] Conventionally, metal-based porous materials are generated by subsequent etching of prefabricated solid alloys; a porous structure of the more noble element arises simultaneously as dissolution of the less noble species is induced chemically or electrochemically.[17,20-25] A single-step approach for the fabrication of multilayer nanowires consisting of alternating porous/solid layers and controlled porosity is presented here. Unlike other methods to create porous nanowires,[12,20] the method is based on directly depositing a porous metal, without involving additional chemical etching or anodization of the less noble alloy component. A AuFe electrolyte was chosen as a model system because the deposition can proceed over a wide range of potential with varying composition, current efficiency, and hence porosity. To the authors' knowledge, fabrication of porous multilayer nanowires by direct electrodeposition has not been achieved before. Gold and iron alloys are electrodeposited from cyanide electrolytes owing to the strong stabilizing ability of these species for metal ions.[12,26-28] As an alternative, a noncyanide electrolyte is developed by replacing the complexant cyanide with a more benign ligand, i.e., citric acid, following the methodology presented by Guan[29] and Guan and Podlaha[30] for analogous AuCo alloys. The resulting electrolyte for Au alloy electrodeposition is similar to that of Valizadeh et al.[28] but without the cyanide species. The parameters for the nanowire deposition were guided by the deposition of thin films onto rotating cylinder electrodes (RCEs).

Experimental

An RCE and polycarbonate (PC) nanoporous membranes were used as working electrodes. For thin-film deposition, the RCE was utilized to characterize the compositional dependence and efficiency of the deposits. The thin films were galvanostatically deposited in a cell with a copper RCE (length of 6 cm and diameter of 0.6 cm), a stationary platinum mesh as a counter electrode (CE), and a reference saturated calomel electrode. The experiments were performed

at three different RCE rotation rates, i.e., 200, 400, and 650 rpm, and the current density was varied in the range of -0.3 and -20 mA/cm^2. Extended deposition times were needed for an accurate composition characterization of thin films obtained at the lowest current densities. The same experimental setup described was also used to generate polarization curves at a sweep rate of 5 mV/s.

The nanowire growth was done using track-etched PC membranes (6 μm thick and 100 nm pore diameter, Osmonics) as templates. The cathode consisted of the PC membrane sputtered on one side with Au and placed inside a poly(ether ketone) holder, whereas a Au anode aligned horizontally to the membrane was the CE. Multilayers were deposited without agitation by current pulses. The nanowires were released from the templates using a dichloromethane bath for 12 h and ultrasonication; solvent removal was achieved by repeated dilution/centrifugation with a high purity ethanol.

The electrolyte solution used for electrodeposition studies and nanowire fabrication consisted of (*i*) citric acid, 0.49 M; (*ii*) FeSO$_4$, 0.29 M; (*iii*) KOH, 1.07 M; and (*iv*) 2.5 mM Au (Techni Gold 25 E). The pH was adjusted to 6.15 with diluted H$_2$SO$_4$ or KOH at room temperature, and deionized ultra filtered water (Fisher Scientific) was utilized for all experiments. Quantitative compositional analysis of the deposits and nanowires was conducted by X-ray fluorescence spectroscopy operating at 45 keV, 2 mA in air with a collimeter of 100 μm in size. Approximately 20 μL of concentrated nanowire suspension was placed in a Cu/carbon-coated transmission electron microscopy (TEM) grid and visualized under a JEOL 1010 TE microscope operating at an accelerating voltage of 60 kV in bright field. Scanning electron microscopy (SEM) images were taken with the aid of a Hitachi S4800 field emission SE microscope operated at 3.0 kV.

The porosity was quantitatively characterized by image analysis (Image J, NIH, Baltimore, MD). Processing of original TEM files consisted of binary image reconstruction at a predetermined grayscale threshold. Approximately 100 in-focus segments were measured to obtain a representative porosity determination, which was calculated as the ratio of void area and total area.

Results and Discussion

Thin films.— The cathodic polarization behavior of the citric acid electrolyte at 200, 400, and 650 rpm and a sweep rate of 5 mV/s is shown in Fig. 1a using the RCE. A region where the potential is affected by the rotation rate was observed between -0.3 and -1.1 V (-0.2 to -10 mA/cm^2). This behavior is indicative of the Au limiting current density; it is expected because this species is maintained at a relatively low concentration in the electrolyte solution (2.5 mM) compared to Fe (0.29 M). Conversely, Fe being present in excess in the solution exhibits a kinetic-controlled behavior in the region examined and is unaffected by the rotation rate.

The composition of the electrodeposits as a function of current

* Electrochemical Society Active Member.
z E-mail: e.podlaha-murphy@neu.edu
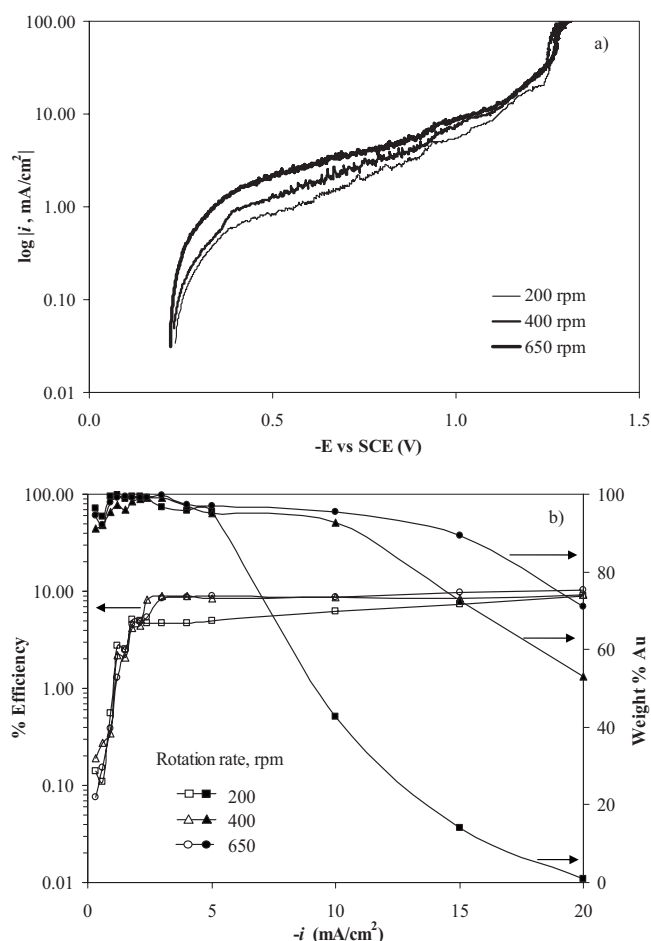
Figure 1. Alloy electrodeposition onto an RCE (a) effect of rotation rate on the polarization behavior at 200 rpm and (b) deposit composition and efficiency.

Figure 2. SEM images of RCE deposits at $i = -10$ mA/cm^2 and 200 rpm.

density and rotation rate (Fig. 1b) indicated the range between -0.9 and -5 mA/cm^2 favorable for Au deposition, whereas FeAu alloys were obtained at higher current densities, becoming richer in Fe with current density. There is a large change in the deposit composition with the rotation rate after an applied current density of -5 mA/cm^2. At high current density, deposits developed a dendritic (porous) appearance. An example of the morphology is shown in SEM images (Fig. 2) at a low (Fig. 2a) and high (Fig. 2b) magnification. The thin film was deposited at -10 mA/cm^2 at a rotation rate of 200 rpm, and the morphology shows pores on the order of 100 nm. The current efficiency was relatively low, between 2 and 10%, in the range of rotation rate and current density studied. At low current densities that current efficiency is very low, then rises and remains steady, between 5 and 10% (Fig. 1b).

Partial current densities as a function of steady-state potential at different rotation rates are shown in Fig. 3. At potentials less negative than -0.7 V, Au deposition is under both diffusion and kinetic control at any rotation rate, whereas in the range of -0.7 and -0.9 V, the partial current density of Au, i_{Au}, shows predominantly a diffusion control behavior and an influence of rotation rate on i_{Au} was observed (Fig. 3a). This diffusional behavior extends from -0.7 to -1.0 V (-0.7 to -1.1 V) at 400 (650) rpm. As the potential became more negative i_{Au} decayed, this effect was, however, less pronounced as the rotation rate increased, and may have been due to the migration of Au ions away from the electrode surface. There was an influence of rotation rate on the partial current of iron, i_{Fe}, at potentials less negative than -0.8 V, whereas at more negative potentials, i_{Fe} becomes less sensitive to variations in rotation rate,
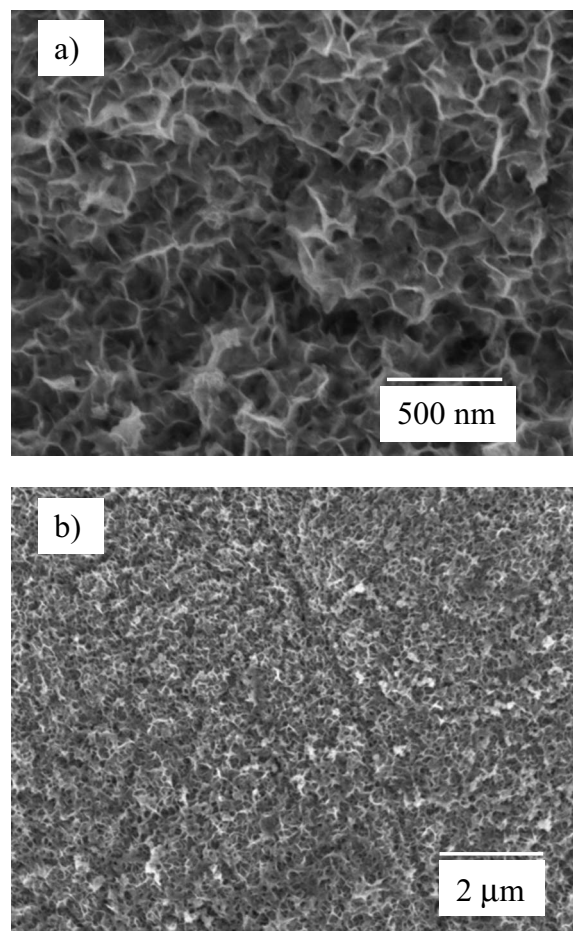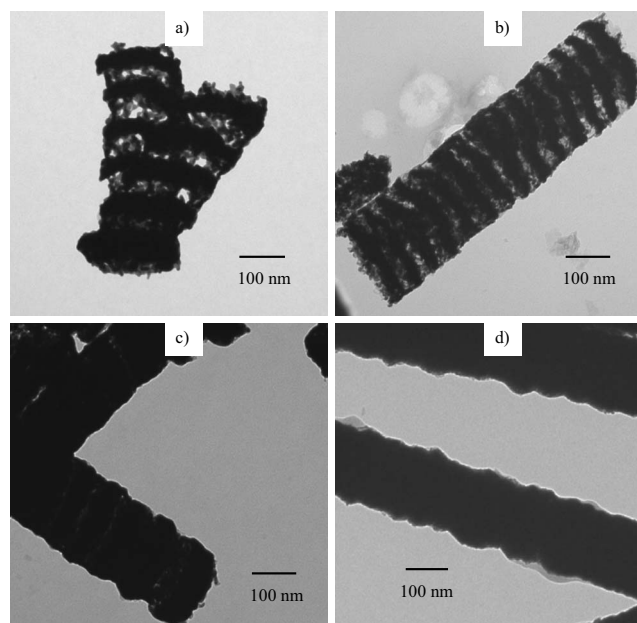
which suggests a mostly kinetically controlled reaction (Fig. 3b). The partial current of side reactions i_{sr} (Fig. 3c) was comparatively high with respect to either i_{Fe} or i_{Au}, which suggested a significant gas evolution in the range of potentials studied.

Nanowire fabrication.— Typical multilayer nanowires fabricated using pulsed galvanic deposition at a current density associated for Au deposition and for a AuFe alloy are shown in Fig. 4. The nanowires were detached from the Au substrate and membrane by breaking them via ultrasound agitation so that only pieces of the nanowires were observed under TEM. They were also ferromagnetic, responding to an external magnet. Different current densities for the alloy layer side (i.e., i_2) were examined. The Au layer was deposited at $i_1 = -0.9$ mA/cm^2, $t_1 = 135$ s, and the alloy was deposited at -10, -12, -15, and -20 mA/cm^2, shown in Fig. 4a-d, respectively, at a deposition time of $t_2 = 25$ s. In Fig. 4a, when the alloy layer was deposited at -10 mA/cm^2, the layer was porous. A significant decrease in porosity was observed by changing the applied current density to more negative values. At an applied current density, $i_2 = -12$ mA/cm^2 (Fig. 4b), the AuFe segments look slightly less porous than in -10 mA/cm^2, whereas at $i_2 = -15$ mA/cm^2 (Fig. 4c), the porous layers were almost indistinguishable, sandwiched within two nonporous dark layers. By changing i_2 to -20 mA/cm^2, both segments appeared solid and only a modulation at the nanowire borders was apparent (Fig. 4d), which suggested that the porosity of the Fe layer disappears at more negative current densities. Compositional analysis of the deposits confirmed that the increase in the applied current density of the porous layer that transitioned into a nonporous layer was accompanied by an increase in Fe.
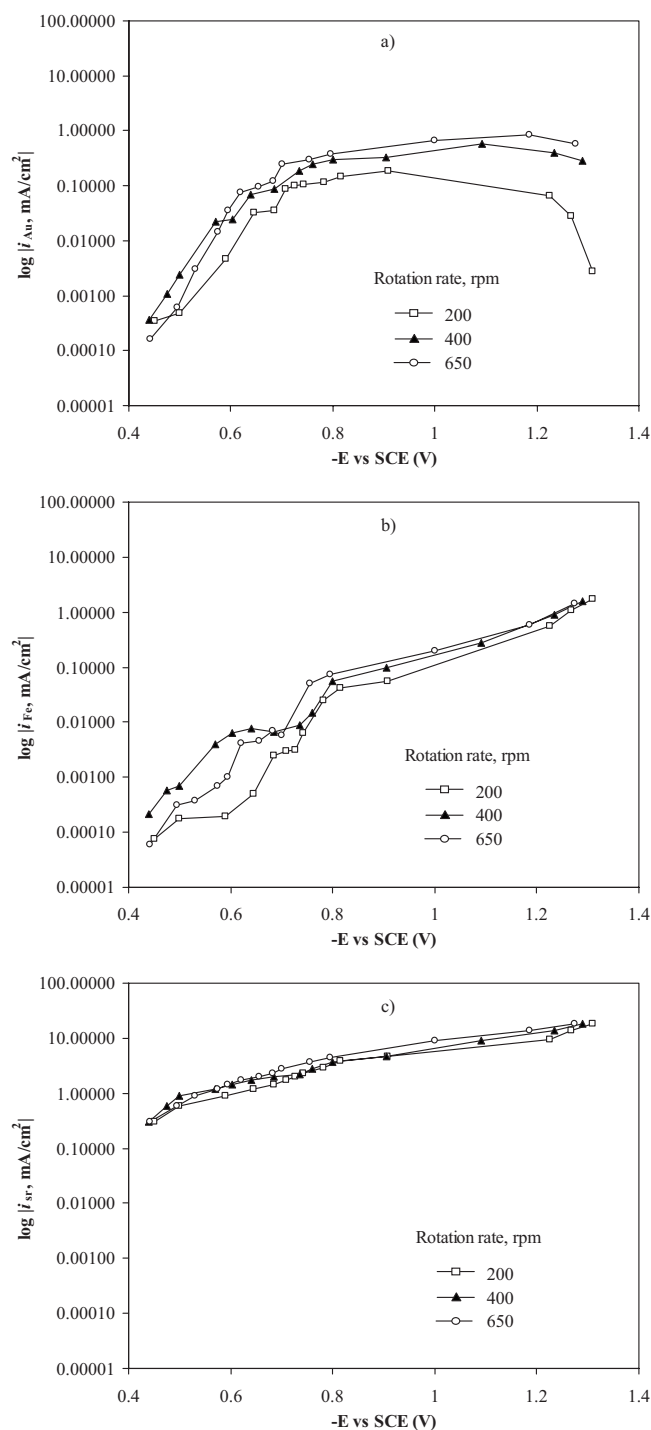
Figure 3. Partial current densities of (a) Au, (b) Fe, and (c) side reactions determined from RCE at 200, 400, and 650 rpm.

Figure 4. Control of porosity in multilayer nanowires by varying the current density i_2: -10, -12, -15, and -20 mA/cm^2 in (a), (b), (c), and (d), respectively; $i_1 = -0.9$ mA/cm^2, $t_1 = 135$ s, and $t_2 = 25$ s in all cases.

Relatively low efficiencies (Fig. 1b) due to an increased i_{sr} (Fig. 3c) contribute to gas bubble formation and may be responsible for the dendritic deposits both in thin films (Fig. 2) and nanowires (Fig. 4 and 5). An efficiency of 14.5% was determined for the AuFe porous layer, which is approximately twice the value determined for the thin film, RCE experiment at 200 rpm (i.e., ~7%, Fig. 1b), suggesting that the deposition occurs in the nanowires in a non-steady-state regime.

A similar trend in the nanowire porosity by increasing only the pulse time of the alloy layer, t_2, is shown in Fig. 6. In all cases, $i_1 = -0.9$ mA/cm^2, $t_1 = 135$ s, and $i_2 = -10$ mA/cm^2, and the pulse times t_2 were 25, 35, 50, and 75 s in Fig. 6a-d, respectively. A decreased porosity was observed by increasing t_2 from 25 to 75 s. At $t_2 = 75$ s, the porous/solid interface was difficult to observe. Upon increasing either current density or deposition time, the charge increases, which suggests that the observed decreased porosity at extended t_2 or i_2 was due to an increase in the total mass deposited. Thicker porous layers did not develop by increasing either i_2 or t_2; this is consistent with a kinetic deposition control of the main reaction (rather than a transport control). According to the partial current density data (Fig. 3) at $|i_2| \geq 10$ mA/cm^2, i.e., $E \leq -1.0$ V, i_{Fe} is
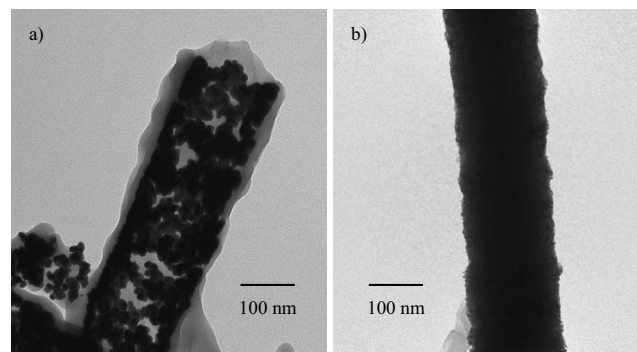
Nanowires in Fig. 5 were deposited by removing one of the layers. Figure 5a shows nanowires that were deposited without the Au layer. The current density was pulsed between $i_1 = 0.0$ mA/cm^2 ($t_1 = 135$ s) and $i_2 = -10$ mA/cm^2 ($t_2 = 25$ s). The resulting deposit was discontinuous and porous. The nanowire in Fig. 5b is a representative example of those fabricated at $i_1 = -0.9$ mA/cm^2 ($t_1 = 135$ s) and $i_2 = 0.0$ mA/cm^2 ($t_2 = 25$ s), eliminating the Fe-rich layer. These nanowires were dense. Thus the porous region is a result of the deposition of the Fe-rich layer, and the Au layer helps to structurally support the porous region.
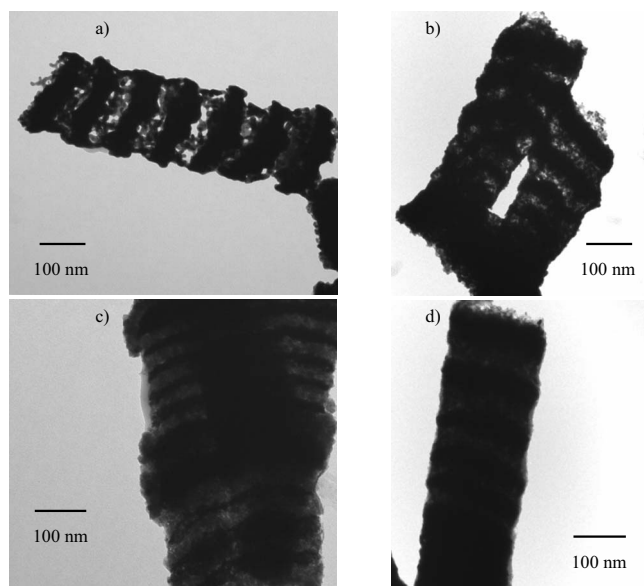

Figure 5. TEM images of nanowires deposited at (a) $i_1 = 0.0$ mA/cm^2 ($t_1 = 135$ s) and $i_2 = -10$ mA/cm^2 ($t_1 = 25$ s) and (b) $i_1 = -0.9$ mA/cm^2 ($t_1 = 135$ s) and $i_2 = 0.0$ mA/cm^2 ($t_1 = 25$ s).

Figure 6. Control of porosity in multilayer nanowires by varying pulse time t_2: 25, 35, 50, and 75 s in (a), (b), (c), and (d), respectively; $i_1 = -0.9$ mA/cm^2, $t_1 = 135$ s, and $i_2 = -10$ mA/cm^2 s in all cases.

mostly under kinetic control; hence the concentration of bulk Fe is uniform within the porous layer and the deposition occurs within the pores rather than at its surface rendering denser layers. An estimate of the predicted change in the nanowire porosity with t_2 and i_2 is presented in the Appendix and captures the qualitative observations in Fig. 4 and 6.

Conclusions

A single-step electrodeposition approach was developed for the synthesis of porous nanowires guided by thin-film experiments. This method was not only advantageous to create porous deposits with alternating solid layers but was also used to modulate porosity as well as composition by varying the conditions of the pulsed current scheme used for their fabrication. A contributing factor for porosity development was gas evolution occurring simultaneously during the electrodeposition process. A predicted decrease with either t_2 or i_2 agreed with qualitative features of the TEM observations.

Acknowledgments

Appendix

Porosity variations with deposition time t_2 can be theoretically estimated from Eq. A-1, which arises from a material balance on the solid phases[31]

$$\frac{\partial \varepsilon}{\partial t_2} = \sum_{\substack{\text{solid} \\ \text{phases}}} \frac{s_i M_i}{\rho_i n F} \nabla \cdot i_{\text{solution}} \qquad [\text{A-1}]$$

Assuming that the reaction is uniform everywhere and all the current transfers from the matrix to the solution phase, then $\nabla \cdot i_{\text{solution}} = a i_n$, where $i_n = i_2$ is the applied current density (A/cm^2) and a is the specific surface area (cm^2/cm^3). As the time proceeds, the surface area per unit volume changes according to Eq. A-2[32] for the case of spherical particles. Thus, changes in porosity ε with time are given by Eq. A-3

$$a = a^0 \left(\frac{1 - \varepsilon}{1 - \varepsilon^0} \right)^{2/3} \qquad [\text{A-2}]$$
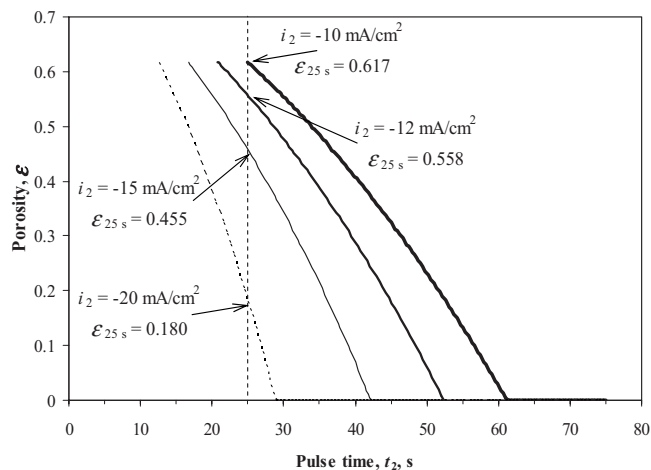
Figure A-1. Influence of pulse time t_2 and applied current density i_2 on predicted porosity of the AuFe layer.

$$\frac{d\varepsilon}{dt_2} = \sum_{\substack{\text{solid} \\ \text{phases}}} \frac{s_i M_i}{\rho_i n F} a^0 \left(\frac{1 - \varepsilon}{1 - \varepsilon^0} \right)^{2/3} i_n \qquad [\text{A-3}]$$

Figure A-1 shows porosity predicted by Eq. A-3 as a function of either pulse time t_2 or applied current density i_2 for the AuFe layer. The contribution of both Au and Fe was taken into account for the estimation of porosity changes by introducing thin-film data shown in Fig. 1b and 2. In all cases, a specific area, $a^0 = 10$ cm^2/cm^3, and a porosity, $\varepsilon^0 = 0.617$ ($t_2 = 25$ s and $i_2 = -10$ mA/cm^2), estimated by quantitative image analysis (Image J) from the TEM were used as initial conditions to the differential equation. This continuum approach hence does not capture the very initial stages of the deposition. In agreement with Fig. 3 and 4, the predicted porosity decreased with either t_2 or i_2, and quantitative ε values (Fig. A-1) showed consistency with qualitative characteristics of images. At an identical applied current density of -10 mA/cm^2, predicted ε were, respectively, 0.48 and 0.22 at $t_2 = 35$ s (Fig. 4b) and $t_2 = 50$ s (Fig. 4c), and the total absence of porosity was reached at $t_2 = 61$ s (Fig. A-1). The effect of the current density i_2 on porosity was determined at constant pulse time, $t_2 = 25$ s, and also shown in Fig. A-1 and assumed a similar starting porosity as -10 mA/cm^2 (0.617) at an early time proportional to the charge in the deposition. The porosity values predicted were slightly overestimated from image characteristics but capture the qualitative features.

References

1. W. Schwarzacher and D. Lashmore, *IEEE Trans. Magn.*, **32**, 3133 (1996).
2. M. Alper, in *Nanostructured Magnetic Materials and Their Applications*, D. Shi, B. Aktas, L. Pust, and F. Mikailov, Editors, p. 111, Springer, Berlin (2002).
3. D. R. Baselt, G. U. Lee, M. Natesan, S. Metzger, P. E. Sheehan, and R. Colton, *Biosens. Bioelectron.*, **13**, 731 (1998).
4. E. L. Edelstein, C. R. Tamanaha, P. E. Sheehan, M. M. Miller, D. R. Baselt, L. J. Whitman, and R. J. Colton, *Biosens. Bioelectron.*, **14**, 805 (2000).
5. J. C. Rife, M. M. Miller, P. E. Sheehan, C. R. Tamanaha, M. Tondra, and L. J. Whitman, *Sens. Actuators, A*, **107**, 209 (2003).
6. Q. Huang and E. J. Podlaha, *J. Electrochem. Soc.*, **151**, C119 (2004).
7. D. Pullini, D. Busquets, A. Ruotolo, G. Innocenti, and V. Amigó, *J. Magn. Magn. Mater.*, **316**, e242 (2007).
8. X.-T. Tang, G.-C. Wang, and M. Shima, *J. Appl. Phys.*, **99**, 123910 (2006).
9. A. Blondel, J. P. Meier, B. Doudin, and J.-Ph. Ansermet, *Appl. Phys. Lett.*, **65**, 3019 (1994).
10. F. Nasirpouri, P. Southern, M. Ghorbani, A. Iraji zad, and W. Schwarzacher, *J. Magn. Magn. Mater.*, **308**, 35 (2007).
11. G. P. Heydon, S. R. Hoon, A. N. Farley, S. L. Tomlinson, M. S. Valera, K. Atten-borough, and W. Schwarzacher, *J. Phys. D*, **30**, 1083 (1997).
12. C. X. Ji and P. C. Searson, *J. Phys. Chem. B*, **107**, 4494 (2003).
13. D. M. Davis, M. Moldovan, D. P. Young, M. Henk, X. Xie, and E. J. Podlaha, *Electrochem. Solid-State Lett.*, **9**, C153 (2006).
14. D. M. Davis, D. Pinisetty, A. Prabhakar, M. Moldovan, D. P. Young, R. Devireddy, M. C. Murphy, and E. J. Podlaha, *ECS Trans.*, **6**(8), 253 (2007).
15. L. Sun, Y. Hao, C.-L. Chien, and P. C. Searson, *IBM J. Res. Dev.*, **49**, 79 (2005).
16. C. Bansal, S. Sarkar, A. K. Mishra, T. Abraham, C. Lemier, and H. Hahn, *Scr. Mater.*, **56**, 705 (2007).
17. M. Guan and E. J. Podlaha, *ECS Trans.*, **3**(25), 347 (2007).
18. S. M. Cohen, *Curr. Opin. Chem. Biol.*, **11**, 115 (2007).
19. P. Horcajada, C. Serre, M. Vallet-Regí, M. Sebban, F. Taulelle, and G. Férey, *Angew. Chem., Int. Ed.*, **45**, 5974 (2006).
20. C. X. Ji and P. C. Searson, *Appl. Phys. Lett.*, **81**, 4437 (2002).
21. A. J. Forty, *Nature (London)*, **282**, 597 (1979).
22. J. Erlebacher, M. J. Aziz, A. Karma, N. Dimitrov, and K. Sieradzki, *Nature (London)*, **410**, 450 (2001).

23. H. W. Pickering and C. Wagner, *J. Electrochem. Soc.*, **114**, 698 (1967).
24. H. W. Pickering, *J. Electrochem. Soc.*, **115**, 143 (1968).
25. H. W. Pickering, *J. Electrochem. Soc.*, **115**, 690 (1968).
26. Y. Okinaka and M. Hoshino, *Gold Bull.*, **31**, 3 (1998).
27. H. Gomathi, *Bull. Electrochem.*, **16**, 459 (2000).
28. S. Valizadeh, E. B. Svedberg, and P. Leisner, *J. Appl. Electrochem.*, **32**, 97 (2002).
29. M. Guan, Ph.D. Thesis, Louisiana State University, Louisiana, MO (2008).
30. M. Guan and E. J. Podlaha, *J. Appl. Electrochem.*, **37**, 549 (2007).
31. J. Newman and K. E. Thomas-Alyea, *Electrochemical Systems*, 3rd ed., p. 536, John Wiley & Sons, Hoboken, NJ (2004).
32. E. J. Podlaha and H. Y. Cheh, *J. Electrochem. Soc.*, **141**, 15 (1994).